Steel and Composite Structures, *Vol. 28, No. 3 (2018) 363-380*
DOI: https://doi.org/10.12989/scs.2018.28.3.363

Analysis of demountable steel and composite frames with semi-rigid bolted joints

Jia Wang [*1], Brian Uy [2a] and Dongxu Li [2b]

[1] *School of Civil and Environmental Engineering, The University of New South Wales, Sydney, NSW 2052, Australia*
[2] *School of Civil Engineering, The University of Sydney, Sydney, NSW 2006, Australia*

(*Received March 13, 2018, Revised May 2, 2018, Accepted May 10, 2018*)

Abstract. This paper presented an integral design procedure for demountable bolted composite frames with semi-rigid joints. Moment-rotation relationships of beam-to-column joints were predicted with analytical models aiming to provide accurate and reliable analytical solutions. Among this, initial stiffness of beam-to-column joints was derived on the basis of Timoshenko's plate theory, and moment capacity was derived in accordance with Eurocodes. The predictions were validated with relevant test results prior to further applications. Frame analysis was conducted by using Abaqus software with material and geometrical nonlinearity considered. Variable lateral loads incorporating wind actions and earthquake actions in accordance with Australian Standards were adopted to evaluate the flexural behaviour of the composite frames. Strength and serviceability limit state criteria were utilized to verify configurations of designed models. A wide range of frames with the varied number of storeys and bays were thereafter programmed to ascertain bending moment envelopes under various load combinations. The analytical results suggest that the proposed approach is capable of predicting the moment-rotation performance of the semi-rigid joints reasonably well. Outcomes of the frame analysis indicate that the load combination with dead loads and live loads only leads to maximum sagging and hogging moment magnitudes in beams. As for lateral loads, wind actions are more crucial to dominate the design of the demountable composite frames than earthquake actions. No hogging moment reversal is expected in the composite beams given that the frames are designed properly. The proposed analysis procedure is demonstrated to be a simple and efficient method, which can be applied into engineering practice.

Keywords: beam-to-column joint; moment-rotation relationship; initial stiffness; moment capacity; demountability; frame analysis

1. Introduction

Blind bolted composite frames have obtained a wide range of investigation and application owing to their significant advantages such as ease of construction, high moment capacity, and ductility as well as excellent seismic resistance (Uy 2012, Ellobody and Young 2015, Hicks and Pennington 2015). The composite structures typically consist of concrete-filled steel tube (CFST) columns and composite beams. The CFST columns are usually connected to steel beams using end-plates as well as blind bolts. Concrete slabs are normally connected to the steel beams by shear connectors. Conventional beam-to-column joints are able to provide sufficient capacity to sustain permanent and imposed actions. However, the frames are difficult to be dismantled in terms of workload and expense since the concrete slabs are bonded with other subassemblies firmly. An innovative design concept that can promote reuse and recycling of steel materials is hence desired. Accordingly, Uy *et al*. (2017) have proposed a blueprint for demountable frames that achieves simple assembly and disassembly by improving structural types of column-to-column joints and beam-to-column joints. The demountable composite column-to-column joints have been investigated by Li *et al*. (2016a, b, 2017), and thus only the demountable beam-to-column joints are discussed in this paper. A related experimental programme has been carried out, and the joint behaviour has been evaluated in a related paper (Wang *et al*. 2018). Even though considerable research topics that focused on the performance of traditional beam-to-column joints have been discussed by Han *et al*. (2008, 2016), Song *et al*. (2017), Yang *et al*. (2015), Jeyarajan and Liew (2016), Nogueiro *et al*. (2009), Beena *et al*. (2017), Ma *et al*. (2011) and Chiew *et al*. (2007), moment-rotation relationships of the innovative joint type in composite frames appear to be still limited. Generally, the demountable joints reduce initial stiffness and moment capacity to some extent compared with the normal ones. Moreover, design codes are not competent to predict the structural performance reasonably well due to the various component characteristics, such as cross-section shapes of columns and joint types. As a result, it requires redesign and recalculation of the composite structures on the basis of sub-model analysis and global frame analysis. The analysis involves the prediction of moment-rotation response of the beam-to-column joints and flexural behaviour of the frame systems under strength limit

*Corresponding author, Ph.D. Student,
E-mail: jia.wang@unsw.edu.au
[a] Professor, E-mail: brian.uy@sydney.edu.au
[b] Ph.D., E-mail: dongxu.li@sydney.edu.au

ISSN: 1229-9367 (Print), 1598-6233 (Online)

state and serviceability limit state.

Loh *et al*. (2006) proposed an analytical model to predict the behaviour of composite flush end-plate joints in terms of the initial stiffness, moment capacity and rotational capacity. By calibrating with experimental results, the simplified and advanced model was able to describe the structural performance reliably and accurately. Similarly, Abolmaali *et al*. (2005) developed moment-rotation equations for steel flush end-plate joints by means of regression analysis. The Ramberg–Osgood model and the three-parameter power model were defined to compare with finite element analysis and test results. Comparison demonstrated that both proposed models had a good agreement with test results. Thai and Uy (2016) extended the application of regression analysis to predict the initial stiffness and moment capacity of bolted joints with hollow or CFST columns. By incorporating a component method outlined from EN 1993-1-8 (2010) and EN 1994-1-1 (2004) into analytical models, the derived empirical equations were proved to be reliable in presenting the joint performance.

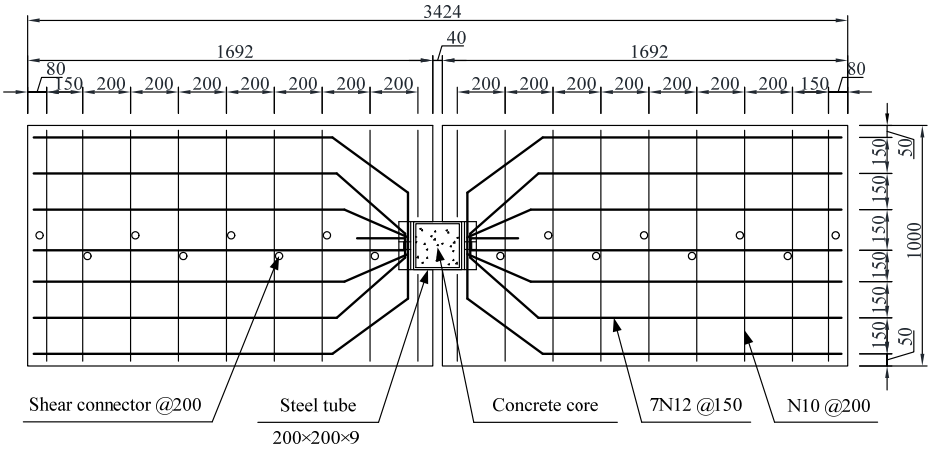

(a) Top view

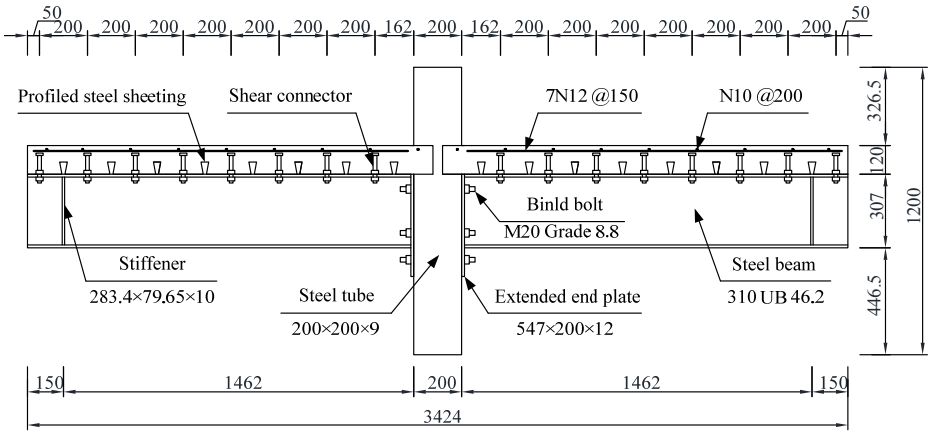

(b) Elevation view

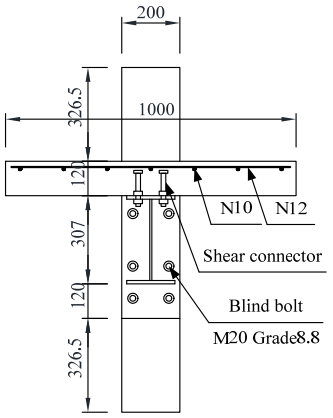

(c) Side view

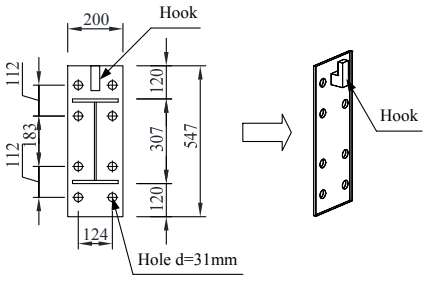

(d) Extended end plate and hook

Fig. 1 Geometry and details of demountable bolted composite joint (units: mm)

Wang (2010) and Gil *et al*. (2013) modified the component method to investigate the flexural behaviour of semi-rigid composite joints. The moment-rotation response in the minor axis direction was incorporated into the overall structural behaviour aiming to revise an overestimation from EN 1993-1-8. In fact, the analytical models mentioned above were limited to some specific configurations where the relevant formulations need to be modified on a case-by-case basis. Besides, some empirical equations were derived by curve fitting that had no practical implications.

As for frame analysis, the global behaviour of composite frames has been investigated extensively. Zhao (2016) developed a nonlinear analysis model which combined shell elements for concrete slabs and discrete beam elements for steel beams to evaluate the flexibility of composite frame systems. The proposed methodology was reported to be viable to provide a precise prediction of the structures. Nie *et al*. (2011) adopted the method to conduct an integrated elasto-plastic analysis of fully connected steel-concrete composite frames. Two critical factors, the slab space composite effect and the beam-column semi-rigidity were incorporated into the model. In comparison with extensive experiments and examples, the proposed model was demonstrated to possess good accuracy and high calculation efficiency. Wang *et al*. (2017a) and Wang *et al*. (2017b) carried out a series of cyclic tests to investigate the seismic behaviour and failure mechanism of two-storey one-bay bolted composite frames. Square and circular columns were taken into consideration separately. Test results revealed that the structural form had a good hysteretic performance and ductility which was able to resist the earthquake efficiently. These studies offered specific design guidance for the bolted steel-concrete frames subjected to monotonic or cyclic loads. However, the nonlinear properties of spring elements simulating bolted beam-to-column joints were rarely considered. Meanwhile, the proposed design guidance was not validated by Australian Standards, and thus it was pending to be applied in the building practice of Australia.

Aiming to address these current issues, a new approach predicting moment-rotation relationships of bolted composite joints was proposed, which incorporated a thin plate theory into the component method. Afterwards, the derived equations of the joints including the initial stiffness and moment capacity were introduced into the composite frame analysis in accordance with Australian design codes. The continuous and integrated procedure is expected to achieve a standardized and simplified design method for engineers in practice.

2. Description of demountable bolted composite joints

The designed composite joints included steel beams that were connected to CFST columns by using extended end plates and a number of blind bolts, details are shown in Fig. 1. Concrete slabs were placed onto the steel beams which accommodated eight high strength bolts acting as shear connectors. To achieve the purpose of demountability, a fundamental design criterion was met to ensure all the components can be dismantled in an easy manner. Accordingly, the discontinuous concrete slabs and reinforcing bars going across the CFST columns were intentionally designed. The bent reinforcements were overlapped through a hook, which was welded to the end-plate in order to transfer tensile stress from the composite beams to the columns. Test results observed by Wang *et al*. (2018) revealed that inner reinforcements were more effective to transfer tensile forces than outer reinforcements. It was due to the fact that the inner reinforcing bars can sustain tension directly, while the outer ones experienced flexural deformations prior to the transfer of forces. The use of blind bolts that connected the extended end-plates and the CFST columns made the assembly more flexible as they can be tightened or removed from outside of the CFST columns with particular tools. Shear connectors between the concrete slabs and the steel beams were made of M20 Grade 8.8 high strength bolts. They were superior to standard welded head studs as they can be unscrewed merely, which rendered the dismantling of the concrete slabs viable. In the structure, the partial shear degree was adopted since it was demonstrated to offer bonding effect between concrete slabs and steel beams sufficiently.

3. Proposed approach for moment-rotation relationship

Prior to the prediction of a moment-rotation relationship of the joints, a series of fundamental theories were introduced and computed referred by Timoshenko's theory (Timoshenko and Woinowsky-Krieger 1959). These theories offered practical solutions to small deformed rectangular plates that were simply supported subjected to partially distributed loads or concentrated loads. Two fundamental assumptions were adopted in this paper.

- Deflections resulting from the applied loads which are perpendicular to a plate surface are small in comparison with the thickness of the plate.
- The edges of the plate are free to move along the thickness plane, any strain in the middle plane of the plate during bending can be ignored.

Based on these assumptions, the differential equation of the deflection surface of the plate subjected to a distributed load can be derived with the details illustrated in Appendices A.1-A.2. Deflections of rectangular plates with varied boundary conditions were thereafter derived in Appendices A.3-A.4. All symbols were summarized in Section Notations.

Afterwards, a specific approach to predict the moment-rotation relationship of the composite joints was recommended. It consisted of two parts, definition of the initial stiffness and the moment capacity. Two assumptions were applied in order to simplify the process.

- Deflections of the CFST column flange in tension resulting from the end-plate in bending were independent.
- Deflections of the CFST column flange in

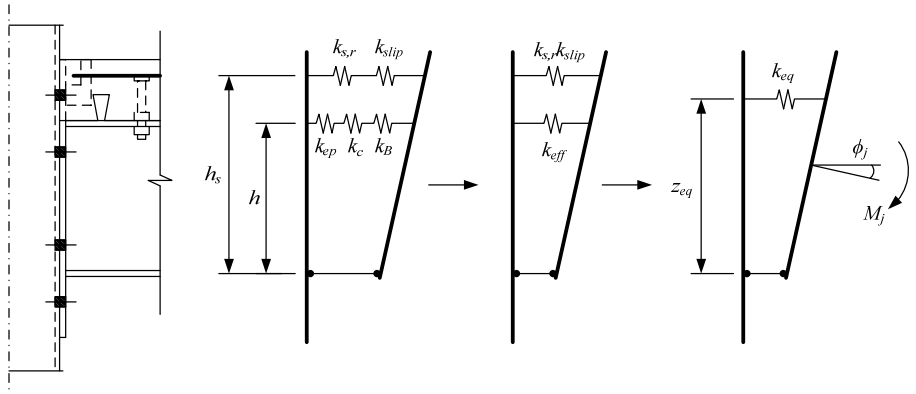

Fig. 2 Stiffness model for a composite bolted joint

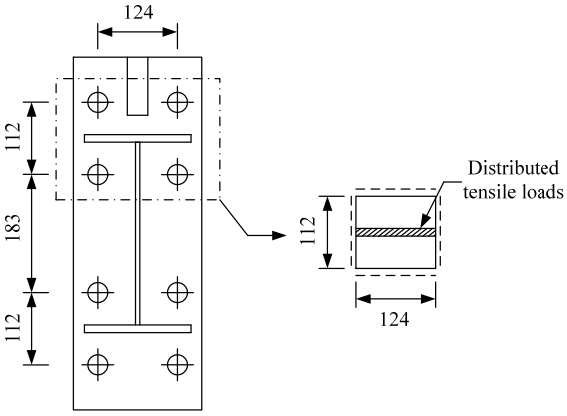

Fig. 3 Geometry of analytical model of end-plate in bending (units: mm)

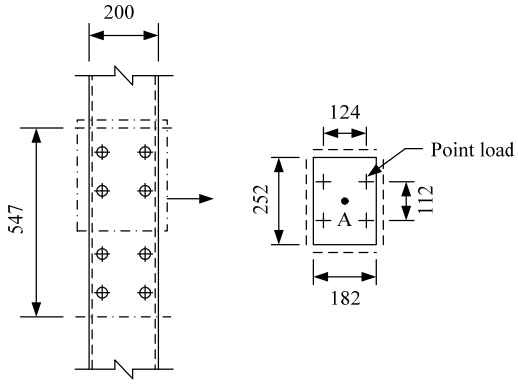

Fig. 4 Geometry of analytical model of column flange in tension (units: mm)

compression and the CFST column web were extremely small that can be ignored.

3.1 Initial stiffness ($S_{j,ini}$)

Fig. 2 illustrates the rotational deformations of a composite joint subjected to hogging moments. The initial stiffness can be obtained by

$$S_{j,ini} = \frac{M_j}{\varphi_j} = \frac{Fz}{\frac{\sum w_i}{z}} = \frac{Fz^2}{\frac{F}{E}\sum\frac{1}{k_i}} = \frac{Ez^2}{\sum\frac{1}{k_i}} \tag{1}$$

It can be seen from Eq. (1), component stiffness k_i depended on the magnitudes of component deflections w_i. On the basis of the assumptions, only four components were taken into account, which included the deflections of the end-plate in bending, CFST column flange in tension, bolts in tension and reinforcements in tension.

The end-plate in bending was regarded as a simply-supported thin plate enclosed by double bolt-rows in tension as indicated in Fig. 3. Meanwhile, the plate was subjected to local distributed tensile loads which were introduced from the beam flange. The effect of beam webs was neglected without any contribution to the locally distributed loads. Deflections of the end-plate can be determined by Eq. (A19). Simultaneously, reactions at the corner of the plate were defined by Eq. (A20) which represented the tensile force applied to the CFST column flange or blind bolts.

Accordingly, deflections of the column flange in tension were mainly caused by prying actions of the end-plate. To simplify the analytical solution, the column flange in tension was considered as a thin plate subjected to four concentrated forces resulting from the corresponding bolts in tension shown in Fig. 4. The equivalent load at each point was equal to the reaction of the end-plate in bending mentioned above. The total deflections of the column flange in tension at point A can be obtained by superimposing the deflections caused by the four point loads.

Likewise, elongations of the bolt shanks can be determined by the reactions. As shown in Fig. 2, the top two bolt rows were considered to compute the deflections. Since values of tensile forces in these bolts were supposed to be identical, the deflections of these four bolts in tension were assumed to be the same and can be denoted by

$$w_{bolt} = \frac{FL_B}{E_B A_B} \tag{2}$$

As for the reinforcements in the demountable composite joints, they were overlapped through the hook welded to the end-plate. Given that the reinforcing bars sustained large tensile loads, the forces were eventually transformed to the end-plate by virtue of the hook. As a result, deflections of

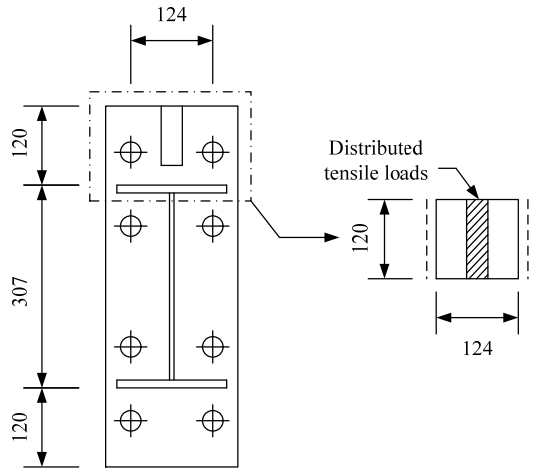

Fig. 5 Geometry of analytical model of reinforcements in tension (units: mm)

the reinforcements can be determined by defining deformations of the end-plate depicted in Fig. 5. In this case, the end-plate was regarded as a thin plate with two opposite edges simply supported and the other two edges free. A uniform distributed load resulting from the reinforcements in tension was applied to the plate. The deflections were solved by Eq. (A29). It should be noted that EN 1994-1-1 highlighted an effect of shear connectors on the stiffness of the reinforcements. A stiffness reduction factor k_{slip} was thus introduced to modify the stiffness coefficient $k_{s,r}$. The expression given in EN 1994-1-1 was denoted by

$$k_{slip} = \frac{1}{1 + \dfrac{E_{s,r}k_{s,r}}{K_{sc}}} \tag{3}$$

with

$$K_{sc} = \frac{Nk_{sc}}{\lambda - \left(\dfrac{\lambda - 1}{1 + \psi}\right)\dfrac{h_s}{d_s}} \tag{4}$$

$$\lambda = \sqrt{\frac{(1+\psi)Nk_{sc}l_b d_s^2}{E_s I_b}} \tag{5}$$

$$\psi = \frac{E_s I_b}{d_s^2 E_{s,r} A_{s,r}} \tag{6}$$

With respect to a composite joint with two bolt-rows in tension, EN 1993-1-8 recommended an option to simplify the stiffness coefficients. Therefore, the initial stiffness in Eq. (1) can be given by

$$S_{j,ini} = \frac{Ez_{eq}^2}{\dfrac{1}{k_{eq}}} \tag{7}$$

with

$$k_{eq} = \frac{k_{eff}h + k_{s,r}k_{slip}h_s}{z_{eq}} \tag{8}$$

$$z_{eq} = \frac{k_{eff}h^2 + k_{s,r}k_{slip}h_s^2}{k_{eff}h + k_{s,r}k_{slip}h_s} \tag{9}$$

$$k_{eff} = \frac{1}{\dfrac{1}{k_{ep}} + \dfrac{1}{k_c} + \dfrac{1}{k_B}} \tag{10}$$

3.2 Moment capacity ($M_{j,pc}$)

EN 1993-1-8 and EN 1994-1-1 specified solutions to define the moment capacities of components which contributed to the plastic behaviour of the joints. In accordance with the design codes, a total of five basic components were considered:

- Reinforcements in tension
- Column flange in bending
- Column web in tension
- Beam web in tension
- Reinforcements in tension

Minimum moment magnitude was selected as the moment capacity of beam-to-column joints. It should be noted that Eurocodes defined the moment capacity based on the yield strength of steel materials rather than the strength at fracture. Therefore, it usually did not correspond to the ultimate moment resistance where the flexural behaviour was governed by steel fractures.

3.3 Nonlinear model for moment-rotation curves

Fig. 6 describes the moment-rotation curve of a composite joint which can be simplified by dividing it into three segments. The first segment was related to the elastic response with a gradient equal to the initial stiffness. The second one was related to the inelastic response, while the last one was related to the strain-hardening response. Ghobarah *et al*. (1996) and Azizinamini *et al*. (1987) suggested that there existed a correlation between the elastic response and the strain-hardening response, namely the stiffness in the strain-hardening stage $S_{j,pc}$ was defined to be $\varphi S_{j,ini}$. The coefficient φ can be varied depending on different structural forms. As a result, a nonlinear analytical model needed to be specified to predict the inelastic response. Two different models were herein adopted to evaluate the moment-rotation behaviour separately recommended by EN 1993-1-8 as well as Yee and Melchers (1986). Results were compared to experimental outcomes, and the optimum prediction was chosen eventually.

EN 1993-1-8 defined the stiffness of the inelastic stage by modifying the initial stiffness

$$S_j = \left(\frac{M_{j,pc}}{1.5M_j}\right)^{2.7} S_{j,ini} \tag{11}$$

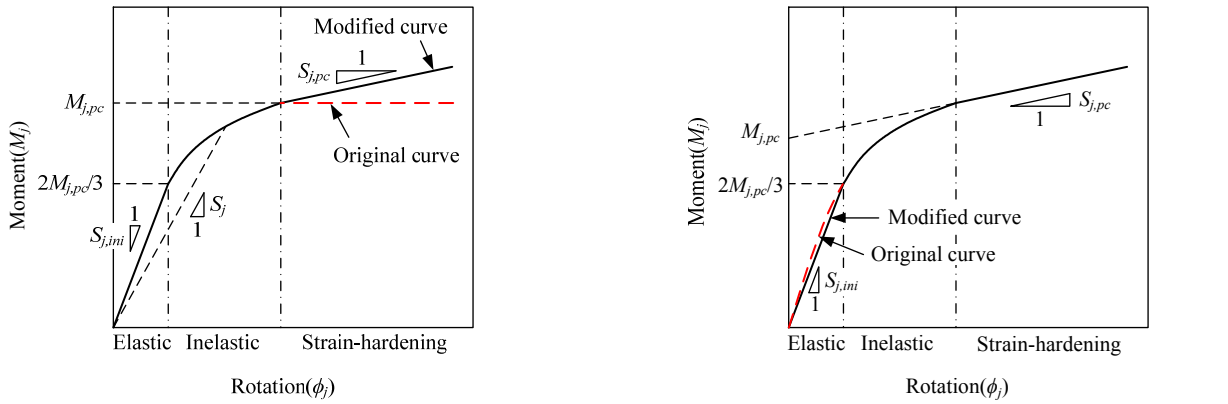

(a) Modified model from EN1993-1-8 (2010) (b) Modified Yee and Melchers model (Yee and Melchers 1986)

Fig. 6 Stiffness model for a composite bolted joint

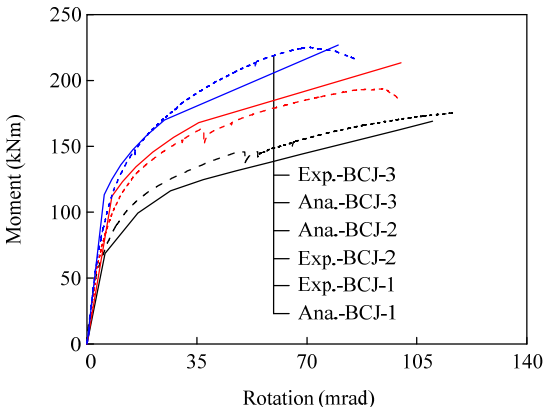

Fig. 7 Validation between tests and analytical models

Table 1 Validation between test results and analytical results

Specimen	Initial stiffness (kN·m/rad)			Ultimate moment resistance (kN·m)		
	$S_{j,ini}$ (Test)	$S_{j,ini}$ (Ana.)	$S_{j,ini}$(Test)/ $S_{j,ini}$(Ana.)	M_u (Test)	M_u (Ana.)	M_u(Test)/ M_u(Ana.)
BCJ-1	11,867	11,997	0.99	174	169	1.03
BCJ-2	14,436	15,237	0.95	194	207	0.94
BCJ-3	22,684	22,126	1.03	225	227	0.99
		Average	0.99			0.99
		SD	0.04			0.05

Meanwhile, the maximum elastic moment resistance in the elastic stage was set as two-thirds of the moment capacity as shown in Fig. 3. With respect to the strain-hardening stage, a modified straight line with a slope of $S_{j,pc}$ being equal to $\varphi S_{j,ini}$ was recommended which was different from the original curve.

The other model proposed by Yee and Melchers (1986) was selected to depict the inelastic stage and the strain-hardening stage, while the elastic behaviour was the same as the model in EN 1993-1-8. The relevant expression was given in Eq. (12).

$$M_j = M_{j,pc} \times \left[1-\exp((-S_{j,ini}+S_{j,pl}-10^5\varphi_j)\frac{\varphi_j}{M_{j,pc}})\right] + S_{j,pl}\varphi_j \quad (12)$$

4. Validation and discussion

The specimens in the research (Wang *et al*. 2018) were selected to validate the accuracy of the proposed model, in which the initial stiffness and moment capacity were formulated on the basis of the theories mentioned above. The comparison is indicated in Fig. 7 and summarized in Table 1. It should be noted that the reinforcements in specimen BCJ-1 were arranged with discontinuous and straight configuration, which were different from specimens BCJ-2 and BCJ-3 with bent reinforcing bars. In this case, the reinforcements in specimen BCJ-1 rarely contributed to the moment moment-rotation response. It is found that the modified moment-rotation curve with Yee and Melchers model for specimen BCJ-1 agreed with the tested results better than that from EN 1993-1-8. On the contrary, the others can adopt the modified model from EN 1993-1-8 aimed to increase the accuracy of predictions.

Overall, the analytical models were capable of predicting the moment-rotation relationship reasonably well. In particular, the predicted curves coincided with the experiments very closely within the elastic stage owing to a fact that the discrepancy of the initial stiffness between the analytical models and the tested specimens was quite tiny. It demonstrated that Timoshenko's plate theory was viable to be used to determine the initial stiffness of the beam-to-column bolted joints.

It is worth noting that the ultimate moment resistance occurred when some components suffered from the fracture. However, the moment capacity in Section 4.2 was determined based on yielding of materials which was less than the maximum moment resistance. It was due to the fact that the yielding of materials was normally not able to result

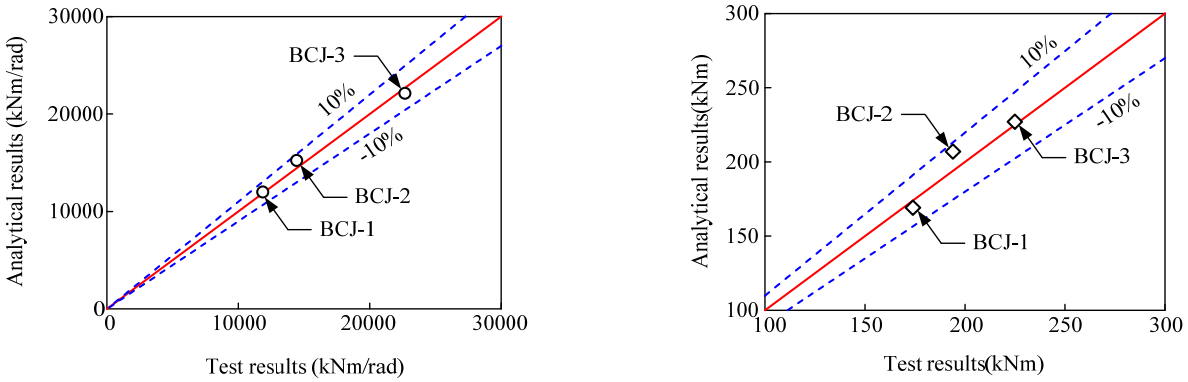

(a) Initial stiffness (b) Ultimate moment resistance

Fig. 8 Comparison between test results and analytical results

in the structural failure in the end. Accordingly, the proposed analytical models cannot experience a descending branch at the strain-hardening stage so that they failed to predict the post-peak behaviour like specimen BCJ-3. Nonetheless, the analytical models were utilized to investigate the frame behaviour of buildings subjected to external design actions in strength limit state. Structural components in these buildings under those design actions cannot achieve fracture or damage. As a result, it is still feasible to apply the predicted models into the frame analysis. Therefore, the rotation capacity was simply taken as a value corresponding to the maximum moment

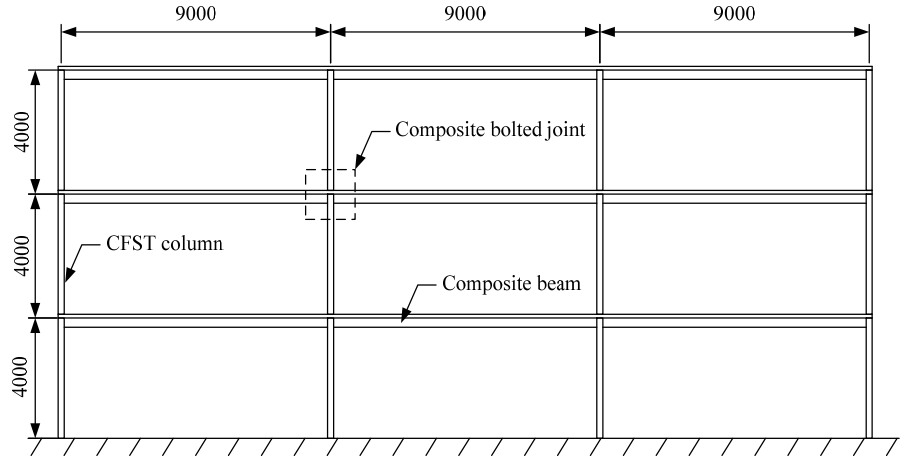

(a) Top view

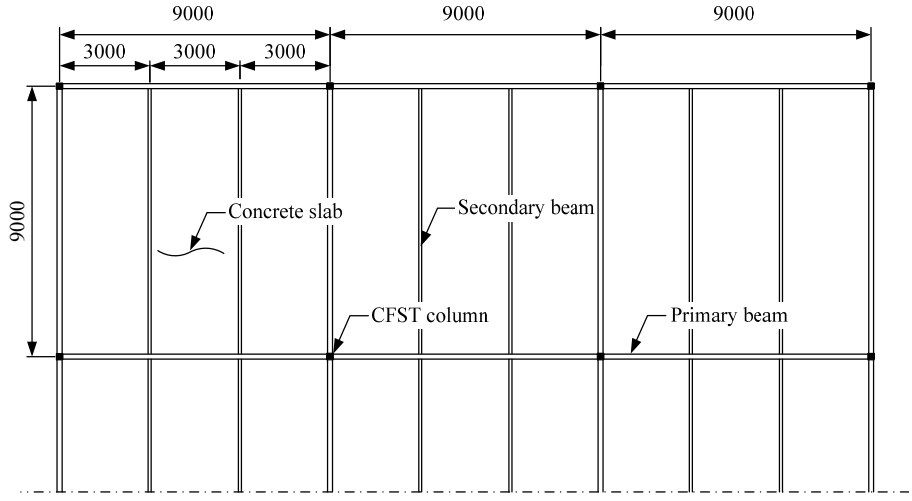

(b) Elevation view

Fig. 9 A composite frame with 3 bays and 3 stories (unit: mm)

resistance. Fig. 8 describes the comparison of initial stiffness and ultimate moment resistance between the test and analytical results. Both demonstrated that the analytical models were reliable to predict the structural performance in a simplified way.

5. Frame analysis

Based on the discussed moment-rotation formulations, it is feasible to develop global models for composite frames by using Abaqus software (Abaqus 2014). Similar to the beam-to-column bolted subassemblies, the frame models were mainly constructed with the CFST columns and the composite beams. The CFST columns were attached to the composite beams by using semi-rigid connection systems. Afterwards, various vertical and lateral design actions which included permanent and imposed actions, earthquake and wind loads were applied to the frames, dedicated to investigating the flexural behaviour of buildings under different scenarios. Since the research was mainly referred to the engineering practice in Australia with moderate seismic actions, low-rise frames less than five stories were hence selected. For simplicity, the frames were considered to possess the same numbers of bays in the orthogonal direction of elevation. Fig. 9 indicates a composite frame structure with three stories and three bays as a case study. It should be noted that the presence of secondary beams and concrete slabs made the out-of-plane rigidity much higher than that in the in-plane direction. In this case, the out-of-plane effect and torsional behaviour of frames can be ignored, and then the three-dimensional frame analysis was reduced to a two-dimensional model in the in-plane direction as shown in Fig. 10.

5.1 Component properties

Plastic behaviour was considered for all components referred to the previous study (Wang *et al*. 2018). There were three major structural subassemblies in the frame including composite beams, composite columns and semi-rigid joints.

5.1.1 Composite beams

Generally, beam elements were preferred in the global models including the composite beams and the CFST columns to reduce computing time. As for the composite beams, the length ratio of hogging moment region to sagging moment region and the cross-section properties were two essential characteristics. EN 1994-1-1 suggested that the length of hogging moment region took up 15%-25% of the beam span, and the value was set as 0.2 in this paper for the frame with semi-rigid joints indicated in Fig. 10. The composite beam section was converted to an equivalent section of steel beam since it was not allowed to define a composite cross section in Abaqus. The equivalent section possessed the same cross-section area, second moment of area and position of neutral axis. Due to the various effective widths of concrete slabs in the hogging moment region and sagging moment region computed by EN 1994-1-1, the conversion of sectional properties was performed separately. Meanwhile, an effect of concrete creeping and shrinkage was taken into consideration for the long-term behaviour of composite beams.

As for hogging and sagging moment regions, EN 1994-1-1 suggested the effective width respectively as follows

$$b_{eff} = b_0 + \frac{0.5L_b}{8} + \frac{0.5L_b}{8} \tag{13}$$

$$b_{eff} = b_0 + \frac{0.7L_b}{8} + \frac{0.7L_b}{8} \tag{14}$$

In this study, the corresponding values can be defined as 1211 mm and 1661 mm, respectively. Also, EN 1998-1 (2004) recommended a different effective width of concrete slab in terms of seismic effects. This was applied to frames subjected to earthquake actions particularly. Accordingly, the effective width for hogging moment regions was set as 1800 mm and that for sagging moment regions was taken as 1350 mm.

5.1.2 Composite columns

Similar to the composite beams, the CFST columns

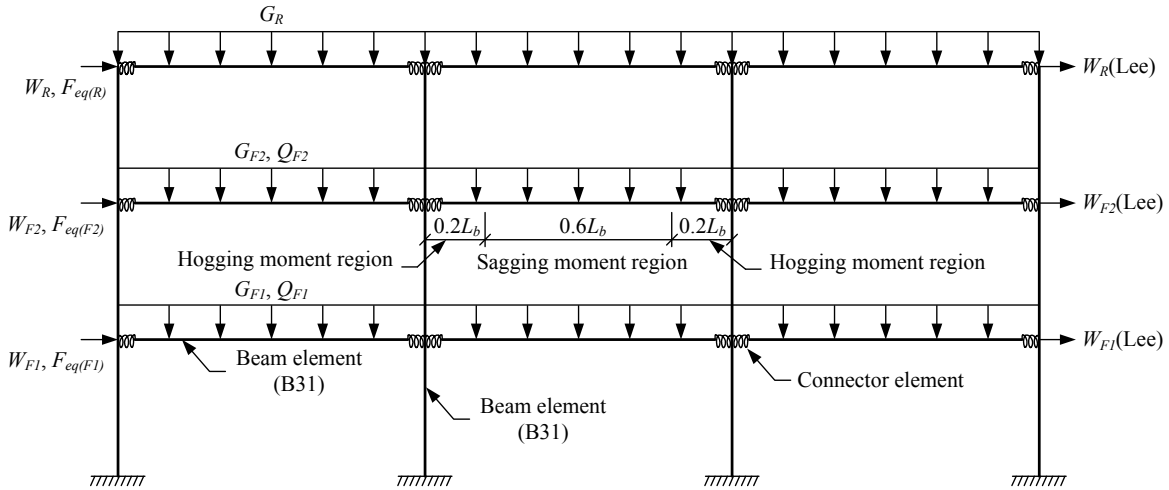

Fig. 10 Finite element model in frame analysis

Table 2 Details of load combination

Number	Strength limit state	Number	Serviceability limit state
LC1	$1.35G$	LC6	$G + 0.7Q$
LC2	$1.2G + 1.5Q$	LC7	$G + 0.4Q$
LC3	$0.9G + W$	LC8	$G + W$
LC4	$1.2G + 0.4Q + W$	LC9	$G + 0.7Q + W$
LC5	$G + 0.3Q + F_{eq}$	LC10	$G + 0.7Q + F_{eq}$

were transformed into equivalent sections by applying the identical effective flexural stiffness and incorporating long-term effects. In accordance with EN 1994-1-1, the effective flexural stiffness of composite columns can be determined by

$$(EI)_{eff} = K_0(E_s I_s + E_{s,r} I_{s,r} + K_e E_{cm} I_c) \tag{15}$$

where K_0 is a correction factor that is taken as 0.5. K_e is a calibration factor that is taken as 0.9.

The columns were fixed to the ground for simplicity which differed from the reality. The degree of flexibility can be disregarded provided that the base connections were designed appropriately. A similar assumption was applied by Thai *et al*. (2016) as well in a frame analysis.

5.1.3 Semi-rigid joints

Design codes classified the beam-to-column joints as pinned connection, semi-rigid connection and rigid connection. Theoretically, the flexural stiffness of the semi-rigid connection was interposed between the pinned and rigid connection. As such, a proper finite element simulating the behaviour of beam-to-column joints was desired to achieve the accurate analysis of frames. Abaqus software provided a powerful element library with various complex properties and yield criteria in which a connector element type HINGE was selected in preference. According to the joint performance, the connector element type can satisfy some requirements that translations were restrained, but the flexural rotation was active. It was superior to spring elements since it was able to simulate pinned, semi-rigid and rigid connection by defining linear, nonlinear and rigid properties. In this study, a moment-rotation relationship was assigned to the connector element to incorporate the plastic behaviour of the semi-rigid joints. The relationship expression based on hogging moments has been abstracted in Section 4. In case that sagging moments appeared around the beam-to-column joints, two sets of moment-rotation data were input for the property of the connector element. The data based on sagging moment were obtained by neglecting the contribution of reinforcements which was similar to the solution of specimen BCJ-1 discussed above.

5.2 Design loads and load combinations

Totally four kinds of loads were included in this study, namely dead loads (G), live loads (Q), wind loads (W) and earthquake loads (F_{eq}) shown in Fig. 10. Table 2 summarizes load combinations in accordance with AS/NZS 1170.0 (2002). oth strength limit state and serviceability limit state were taken into consideration. All load conditions were taken to impose adverse influence on frames.

Table 3 Actual values of actions in frames

Storey	Dead load (kN/m)	Live load (kN/m)	Wind actions (kN)		Earthquake actions (kN)
			Windward	Leeward	
First storey	18.2	22.5	43.5	23.6	24
Second storey	18.2	22.5	43.5	23.6	48
Third storey	13.7	0	21.8	11.8	40.3

According to AS/NZS 1770.1 (2002), the dead loads consisted of self-weight of concrete slabs and steel beams. At the same time, a superimposed dead load of 1 kPa was assumed as well to incorporate additional structure. Office loading was chosen as the live load of 5 kPa. For simplicity, there was no concentrated load applied on floors or roofs. In addition, roofs of frames were merely subjected to dead loads.

As for wind loads acting perpendicularly to walls of structures, a wind speed with a 50-year design working life and 1/500 annual probability of exceedance was herein defined referred by AS/NZS 1770.2 (2011). This almost represented the most adverse condition to a broad region in Australia. The wind pressure was then determined to incorporate the windward and leeward wind. Afterwards, it was converted into equivalent point loads applied to the frame on each level shown in Fig. 10.

Likewise, the actions resulting from earthquakes were obtained from AS/NZS 1170.4 (2007) based on a principle of 50-year design working life and 1/1000 annual probability of exceedance. To achieve an adverse load that reflected a practical and critical seismic condition in Australia, an assumption with sub-soil Class D and Earthquake Design Category II was proposed. The corresponding point loads were then computed and distributed on the frame shown in Fig. 10.

The specific design loads are outlined in Table 3 where a three-storey frame was taken for an example.

5.3 Basic analysis procedures

Fig. 11 describes a simple procedure of frame analysis starting from the determination of component dimensions. Aiming to achieve specific frame details in terms of dimension and configuration of components, the criteria for serviceability limit state and ultimate limit state was utilized to verify analysis results. In fact, the beam-to-column composite frame was designed by trial and error which guaranteed an ideal structure without oversized members. AS/NZS 1170 recommended the mid-span deflection limit of composite beams was $L_b/250$, whereas the inter-storey drift limit of columns was $H_c/150$ for wind actions in serviceability limit state and 1.5% for earthquake actions in ultimate limit state. Besides, EN 1993-1-1 (2005) suggested

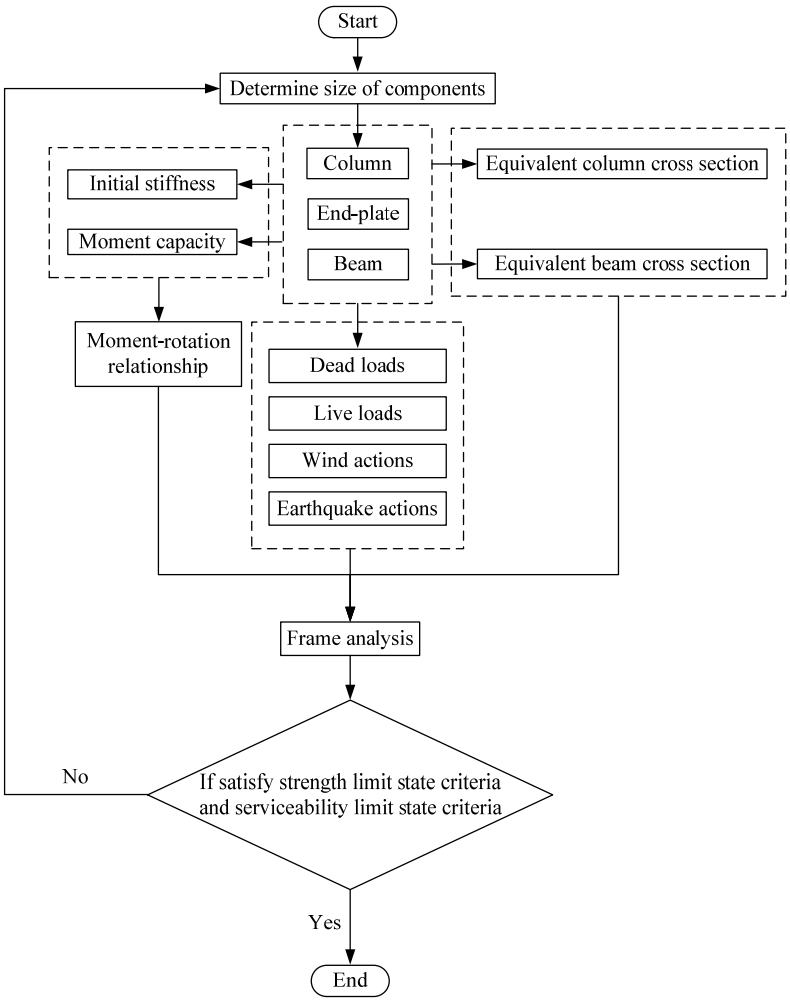

Fig. 11 Flowchart of frame analysis

more strict design criteria for columns where the inter-storey drift limit of columns reached $H_c/300$ in serviceability limit state. It was adopted in this study.

A three-storey by three-bay frame with an assumed size of columns and beams was first verified if it satisfied the strength and serviceability limit state criteria. Otherwise, the frame was redesigned, and the moment-rotation relationship of the joints was regenerated. The analysis procedure was repeated until a flexible frame configuration was achieved.

5.4 Results and discussions

Fig. 12 illustrates the frame results under load combinations in strength limit state. The results were checked on the basis of strength limit state criteria and serviceability limit state criteria. The sagging and hogging bending moments in beams were highlighted and indicated in Figs. 13 and 14 since they were the prime studied parameters. The selected column cross section was 400 × 400 × 16 mm, while the beam was 310UB46.2 and the depth of concrete slab was 120 mm. It can be seen that LC2 incorporating dead loads and live loads was more critical to the frame in terms of sagging bending moments. Meanwhile, the frame achieved maximum hogging moment values under the same load combination. It should be noted that the ratio of hogging moments to sagging moments here reached over 0.4. As for full-rigid and pinned joints under uniformly distributed loads, the corresponding ratio was 2 and 0, respectively. It was expected since the semi-rigid joints sustained less hogging moments than the rigid ones. In comparison with wind actions and earthquake actions, the former imposed more significant influence on the composite bolted frames in Australia where wind was more adverse than earthquake. The analysis results also suggested that the extremum value of sagging moments and hogging moments majorly appeared on the ground floor close to the windward or earthquake actions. It can be deduced that the structure in the ground floor and at the end span was crucial to control the design.

The moment-rotation relationship of the semi-rigid joints was indicated in Fig. 15. The results were abstracted from the frame under LC2 where maximum hogging moments occurred. It can be found that the bolted joints experienced plastic response, and the hogging moment reached 177 kN·m which took up 69% of the ultimate moment resistance. On the other hand, the hogging moment decreased when lateral loads were applied to the frame.

The frame analysis was then extended to a wide range where the storey varied from two to five and the bay shifted

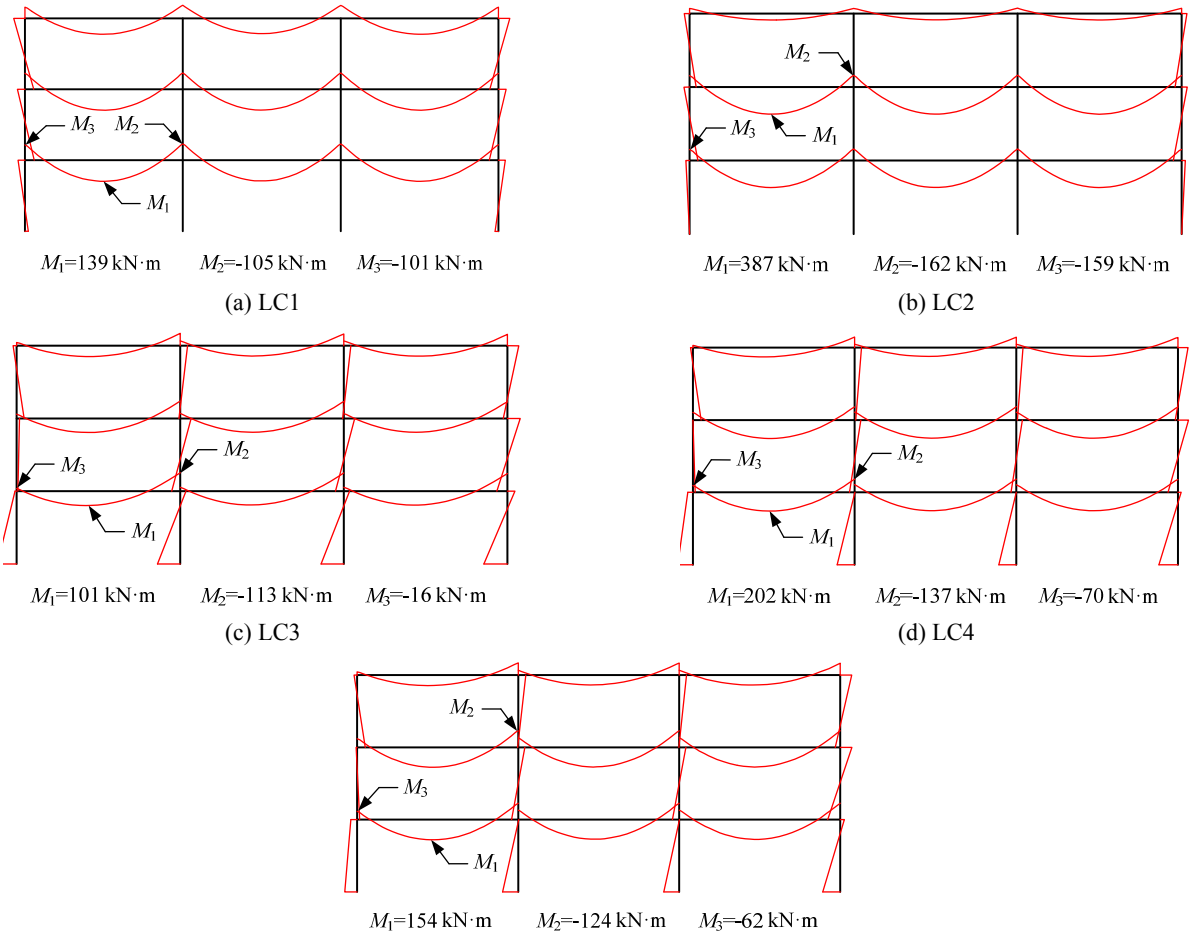

Fig. 12 Bending moment diagrams in strength limit state

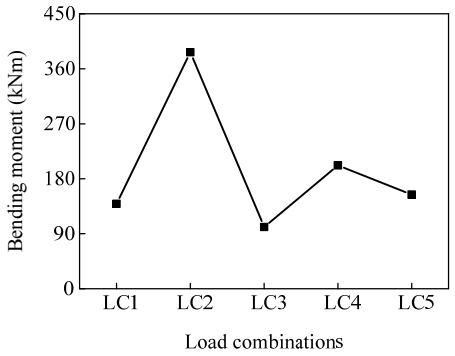

Fig. 13 Maximum sagging moment of composite beams

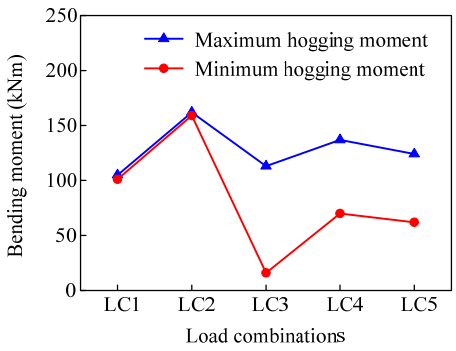

Fig. 14 Hogging moment of composite joints

between two and four. Tables 4 and 5 summarize the sagging moment and hogging moment envelopes under load combinations. The analysis results revealed that the maximum sagging and hogging moments happened in LC2, while the minimum sagging and hogging moments appeared in LC3. It can be further implied that wind actions rather than earthquake actions dominated the design of composite bolted frames. As for minimum hogging bending moments shown in Fig. 16, the values were not reversed in most cases. It suggested that the beam-to-column joints can be designed without moment reversal considered due to lateral loads if a structural form was properly proposed. To achieve this, the frame was generally designed with less than five storeys, and more bays should benefit the construction.

In addition, the effective width of beam segments adjacent to columns was determined under hogging moment conditions by default. This means the beam-to-column joints have been assumed to be subjected to hogging moments before frame analysis. However, the assumption cannot comply with some cases that sagging moments appeared at the joints since the effective width was not able

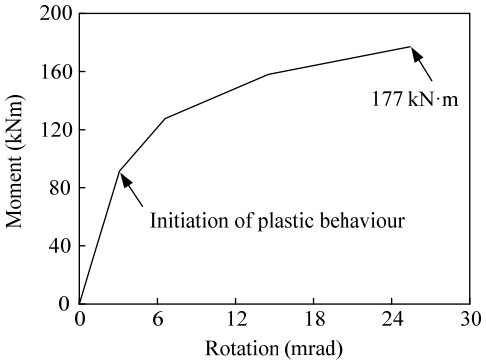

Fig. 15 Validation between tests and analytical models

Table 4 Sagging bending moment envelope in strength limit state

	Sagging bending moment (unit: kN·m)		
	2 bays	3 bays	4 bays
2 storeys	385(94)*	385(93)	384(93)
3 storeys	387(110)	387(101)	387(97)
4 storeys	387(159)	387(158)	387(158)
5 storeys	387(159)	387(158)	387(158)

* Data in and out of brackets represent minimum and maximum sagging bending moments

Table 5 Hogging bending moment envelope in strength limit state

	Hogging bending moment (unit: kN·m)		
	2 bays	3 bays	4 bays
2 storeys	160(34)*	160(43)	160(49)
3 storeys	162(3)	162(16)	162(28)
4 storeys	163(-31**)	163(5)	163(24)
5 storeys	165(-41)	162(-26)	162(3)

* Data in and out of brackets represent minimum and maximum hogging bending moments

** Data with negative sign represent sagging bending moments

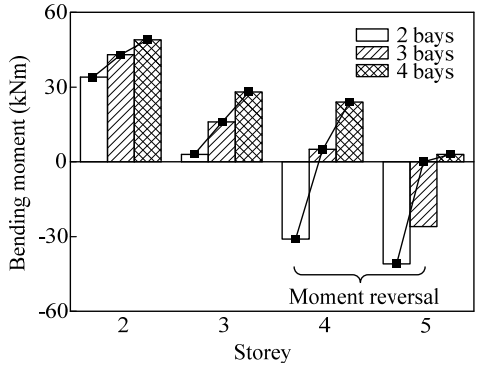

Fig. 16 Minimum hogging moments in frames

to switch into the value defined by sagging moments during computation. Therefore, the study is limited to frames in which beam-to-column joints only experience hogging moments. The limit is reasonable and to be expected as the design form is ideal for beam-to-column joints under hogging moments. As mentioned above, the purpose can be achieved viably provided that an appropriate design is guaranteed.

6. Conclusions

The study elaborated the behaviour and design of demountable bolted composite frames with semi-rigid joints. A method for determining the moment-rotation relationship of joints was proposed which was validated with relevant tested results. The definition of initial stiffness was based on Timoshenko's plate theory that provided a straightforward approach to solve rotations of beam-to-column joints. The prediction was then applied to the frame analysis where two-dimensional finite element models incorporating material nonlinearity and second-order effects were developed. Load combinations including dead loads, live loads, wind actions and earthquake actions under strength limit state and serviceability limit state were employed. The demountable composite bolted frames were designed by verifying strength and serviceability limit state criteria.

The proposed analytical model is able to predict the moment-rotation relationship of composite bolted joints with high accuracy. Timoshenko's plate theory is liable to be used to determine the initial stiffness of the structures.

The advanced frame analysis is an effective way to design the demountable composite frames that satisfy strength and serviceability limit state criteria. Meanwhile, it is convenient to identify the critical loading conditions that influence the structural behaviour. Accordingly, the combination of dead loads and live loads was considered to affect the frame significantly in terms of bending moments in composite beams. Analysis results suggest that wind actions are more adverse to the structures than earthquake actions. In addition, no moment reversal occurs in the hogging moment region provided that the frames are designed properly. In this case, the configuration of demountable beam-to-column joints can be simple. The proposed analysis procedure is applicable to engineering practice addressing variable issues in a proper and efficient manner.

Acknowledgments

The research described in this paper is financially supported by the Australian Research Council (ARC) under its Discovery Scheme (Project No: DP140102134). The corresponding author is financially support by Australian Government Research Training Program Scholarship. Both are gratefully acknowledged.

References

Abaqus (2014), User Manual; Version 6.14, DS SIMULIA Corp., Providence, RI, USA.

Abolmaali, A., Matthys, J.H., Farooqi, M. and Choi, Y. (2005), "Development of moment-rotation model equations for flush end-plate connections", *J. Constr. Steel Res.*, **61**(12), 1595-1612.

AS/NZS 1170.0-2002 (2002), Structural design actions. part 0: general principles; Australia.

AS/NZS 1170.1-2002 (2002), Structural design actions. part 1: permanent, imposed and other actions; Australia.

AS/NZS 1170.2-2011 (2011), "Structural design actions. part 2: wind actions", Australia.

AS/NZS 1170.4-2007 (2007), "Structural design actions. Part 4: Earthquake actions in Australia", Australia.

Azizinamini, A., Bradburn, J.H. and Radziminski, J.B. (1987), "Initial stiffness of semi-rigid steel beam-to-column connections", *J. Constr. Steel Res.*, **8**, 71-90.

Beena, K., Naveen, K. and Shruti, S. (2017), "Behaviour of bolted connections in concrete-filled steel tubular beam-column joints", *Steel Compos. Struct., Int. J.*, **25**(4), 443-456.

Chiew, S.P., Lee, C.K., Lie, S.T. and Ji, H.L. (2007), "Fatigue behaviors of square-to-square hollow section T-joint with corner crack. I: Experimental studies", *Eng. Fract. Mech.*, **74**(5), 703-720.

Ellobody, E. and Young, B. (2015), "Nonlinear analysis of composite castellated beams with profiled steel sheeting exposed to different fire conditions", *J. Constr. Steel Res.*, **113**, 247-260.

EN 1993-1-1 (2005), Eurocode 3: Design of steel structures. part 1–1: general rules and rules for buildings; European Committee for Standardization, Brussels, Belgium.

EN 1993-1-8 (2010), "Eurocode 3: Design of steel structures. part 1–8: design of joints", European Committee for Standardization, Brussels, Belgium.

EN 1994-1-1 (2004), "Eurocode 4: Design of composite steel and concrete structures. part 1–1: general rules and rules for buildings", European Committee for Standardization, Brussels, Belgium.

EN 1998-1 (2004), "Eurocode 8: Design of structures for earthquake resistance. part 1: general rules, seismic actions and rules for buildings", European Committee for Standardization, Brussels, Belgium.

Ghobarah, A., Mourad, S. and Korol, R.M. (1996), "Moment-rotation relationship of blind bolted connections for HSS columns", *J. Constr. Steel Res.*, **40**(1), 63-91.

Gil, B., Goni, R. and Bayo, E. (2013), "Experimental and numerical validation of a new design for three-dimensional semi-rigid composite joints", *Eng. Struct.*, **48**, 55-69.

Han, L.H., Wang, W.D. and Zhao, X.L. (2008), "Behaviour of steel beam to concrete-filled SHS column frames: Finite element model and verifications", *Eng. Struct.*, **30**(6), 1647-1658.

Han, C., Li, Q., Wang, X., Jiang, W. and Li, W. (2016), "Research on rotation capacity of the new precast concrete assemble beam-column joints", *Steel Compos. Struct., Int. J.*, **22**(3), 613-625.

Hicks, S.J. and Pennington, A. (2015), "Partial factors for the design resistance of composite beams in bending", *J. Constr. Steel Res.*, **105**(2), 74-85.

Jeyarajan, S. and Liew, J.Y.R. (2016), "Robustness analysis of 3D Composite buildings with semi-rigid joints and floor slab", *Structures*, **6**, 20-29.

Li, D.X., Uy, B., Patel, V. and Aslani, F. (2016a), "Behaviour and design of demountable steel column-column connections", *Steel Compos. Struct., Int. J.*, **22**(2), 429-448.

Li, D.X., Uy, B., Aslani, F. and Patel, V. (2016b), "Analysis and design of demountable steel column-baseplate connections", *Steel Compos. Struct., Int. J.*, **22**(4), 753-775.

Li, D.X., Uy, B., Patel, V. and Aslani, F. (2017), "Analysis and design of demountable embedded steel column base connections", *Steel Compos. Struct., Int. J.*, **23**(3), 303-315.

Loh, H.Y., Uy, B. and Bradford, M.A. (2006), "The effects of partial shear connection in composite flush end plate joints - Part II - Analytical study and design appraisal", *J. Constr. Steel Res.*, **62**(4), 391-412.

Ma, H.W., Jiang, W.S. and Cho, C. (2011), "Experimental study on two types of new beam-to-column connections", *Steel Compos. Struct., Int. J.*, **11**(4), 291-305.

Nogueiro, P., Silva, L.S.D., Bento, R. and Simões, R. (2009), "Calibration of model parameters for the cyclic response of end-plate beam-to-column steel-concrete composite joints", *Steel Compos. Struct., Int. J.*, **9**(1), 39-58.

Nie, J.G., Tao, M.X., Cai, C.S. and Chen, G. (2011), "Modeling and investigation of elasto-plastic behavior of steel-concrete composite frame systems", *J. Constr. Steel Res.*, **67**(12), 1973-1984.

Song, T.Y., Tao, Z., Razzazzadeh, A., Han, L.H. and Zhou, K. (2017), "Fire performance of blind bolted composite beam to column joints", *J. Constr. Steel Res.*, **132**(5), 29-42.

Thai, H.T. and Uy, B. (2016), "Rotational stiffness and moment resistance of bolted endplate joints with hollow or CFST columns", *J. Constr. Steel Res.*, **126**, 139-152.

Thai, H.T., Uy, B., Kang, W.H. and Hicks, S. (2016), "System reliability evaluation of steel frames with semi-rigid connections", *J. Constr. Steel Res.*, **121**, 29-39.

Timoshenko, S. and Woinowsky-Krieger, S. (1959), *Theory of Plates and Shells*, (2nd Edition), McGraw-Hill, New York, NY, USA.

Uy, B. (2012), "Applications, behaviour and design of composite steel-concrete structures", *Adv. Struct. Eng.*, **15**(9), 1559-1571.

Uy, B., Patel, V., Li, D.X. and Aslani, F. (2017), "Behaviour and design of connections for demountable steel and composite structures", *Structures*, **9**, 1-12.

Wang, A.J. (2010), "A study on composite end-plate connections with flexible tensile reinforcements and shear connectors", *Can. J. Civil Eng.*, **37**(11), 1437-1450.

Wang, J., Uy, B., Thai, H.T. and Li, D.X. (2018), "Behaviour and design of demountable beam-to-column composite bolted joints with extended end-plates", *J. Constr. Steel Res.*, **144**, 221-235.

Wang, J., Pan, X. and Peng, X. (2017a), "Pseudo-dynamic tests of assembly blind bolted composite frames to CFST columns", *J. Constr. Steel Res.*, **139**, 83-100.

Wang, J.F., Li, B.B., Wang, D.H. and Zhao, C.F. (2017b), "Cyclic testing of steel beam blind bolted to CFST column composite frames with SBTD concrete slabs", *Eng. Struct.*, **148**(10), 293-311.

Yang, B., Tan, k.H. and Xiong, G. (2015), "Behaviour of composite beam–column joints under a middle-column-removal scenario: Component-based modelling", *J. Constr. Steel Res.*, **104**, 137-154.

Yee, Y.L. and Melchers, R.E. (1986), "Moment-Rotation Curves for Bolted Connections", *J. Struct. Eng.*, **112**(3), 615-635.

Zhao, H. (2016), "Analysis of seismic behavior of composite frame structures", *Steel Compos. Struct., Int. J.*, **20**(3), 719-729.

DL

Notation

A_B Cross-section area of blind bolt shank
$A_{s,r}$ Cross-section area of reinforcing steel
D Flexural rigidity (equals to $E\delta^3/(12(1-\nu^2))$)
E Young's Modulus
E_B Design value of modulus of elasticity of blind bolts
E_s Design value of modulus of elasticity of structural steel
E_{cm} Design value of modulus of elasticity of concrete
$E_{s,r}$ Design value of modulus of elasticity of reinforcing steel
$(EI)_{eff}$ Effective flexural stiffness of composite columns
F Load applied on beam flanges or a sum of partial distributed loads applied on thin plates
F_{eq} Earthquake actions
F_R Reactions on simply-supported thin plates
G Dead loads
H_c Height of inter-storey columns
I_b Second moment of area of beam's section
I_c Second moment of area of infilled concrete core
I_s Second moment of area of steel tube
K_0 Correction factor
K_e Calibration factor
L_B Clear space of blind bolt shanks between bolt heads and nuts
L_b Span of beams between columns
M_x, M_y Bending moments on thin plates
M_{xy}, M_{yx} Twisting moments on thin plates
M_j Bending moment of beam-to-column joints
$M_{j,pc}$ Moment capacity of beam-to-column joints
N Number of shear connectors distributed over hogging moment regions
Q Live loads
Q_x, Q_y Shear forces on thin plates
S_j Stiffness of beam-to-column joints
$S_{j,ini}$ Initial stiffness of beam-to-column joints
$S_{j,pc}$ Strain-hardening stiffness of beam-to-column joints
W Wind actions
a, b Length and width of rectangular plates
b_{eff} Effective width of concrete slab
b_0 Distance between centres of outstand shear connectors
d_s Distance between longitudinal reinforcing bars in tension and centroid of beam's section
h Distance between centroid of beam flanges in tension and centroid of beam flanges in compression
h_s Distance between longitudinal reinforcing bars in tension and centroid of beam flanges in compression
k_B Stiffness coefficient for blind bolts
k_c Stiffness coefficient for column walls
k_{eff} Effective stiffness coefficient for basic components including end-plates, column walls and blind bolts
k_{ep} Stiffness coefficient for end-plates
k_{eq} Equivalent stiffness coefficient for beam-to-column joints
k_i Stiffness coefficient for basic components
k_{sc} Stiffness coefficient for shear connectors
k_{slip} Reduction factor of stiffness coefficient $k_{s,r}$
$k_{s,r}$ Stiffness coefficient for reinforcing bars
l_b Length of beams on hogging bending moment regions
m, n Positive integers
q Distributed loads on rectangular plates
w Deflections of rectangular plates
w_{bolt} Elongation of blind bolt shanks
w_i Deflections of basic components
z Lever arm
z_{eq} Equivalent lever arm
α_m Equals to $m\pi y/a$.
δ Thickness of thin plates
ν Poisson's ratio
φ Factor of initial stiffness
ϕ_j Rotational deformations of beam-to-column joints

Appendix A

A.1 Determination of internal forces and moments in the middle plane of the plate (*Timoshenko 1959*)

As shown in Fig. A1(a), based on the three dimensional geometric equations and mechanical equations, the components of strain in a hexahedron abstracted from the thin plate with a thickness being δ can be obtained

$$\begin{aligned}
&\varepsilon_x=\frac{\partial u}{\partial x}=\frac{1}{E}[\sigma_x-\nu(\sigma_y+\sigma_z)], \quad \gamma_{yz}=\frac{\partial w}{\partial y}+\frac{\partial v}{\partial z},\\
&\varepsilon_y=\frac{\partial v}{\partial y}=\frac{1}{E}[\sigma_y-\nu(\sigma_z+\sigma_x)], \quad \gamma_{zx}=\frac{\partial u}{\partial z}+\frac{\partial w}{\partial x},\\
&\varepsilon_z=\frac{\partial w}{\partial z}=\frac{1}{E}[\sigma_z-\nu(\sigma_x+\sigma_y)], \quad \gamma_{xy}=\frac{\partial v}{\partial x}+\frac{\partial u}{\partial y}.
\end{aligned} \tag{A1}$$

Since any strain in the middle plane of the plate was assumed to be neglected, ε_z=0, γ_{zx}=0, γ_{yz}=0 can be adopted. Therefore, Eq. (A1) was revised

$$\begin{aligned}
&\frac{\partial u}{\partial z}=-\frac{\partial w}{\partial x}, \qquad \frac{\partial v}{\partial z}=-\frac{\partial w}{\partial y},\\
&\varepsilon_x=\frac{1}{E}(\sigma_x-\nu\sigma_y), \quad \varepsilon_y=\frac{1}{E}(\sigma_y-\nu\sigma_x),\\
&\gamma_{xy}=\frac{1}{E}(1+\nu)\tau_{xy}.
\end{aligned} \tag{A2}$$

For the case when no displacements that were parallel to the middle plane occurred, the deflections w were the function with respect to x and y. Integrating displacements u and v in Eq. (A2), it was found

$$u=-\frac{\partial w}{\partial x}z, \qquad v=-\frac{\partial w}{\partial y}z. \tag{A3}$$

Substitute Eq. (A3) into Eq. (A1) to transform strains into the equations with respect to deflections w

$$\varepsilon_x=-\frac{\partial^2 w}{\partial x^2}z, \quad \varepsilon_y=-\frac{\partial^2 w}{\partial y^2}z, \quad \gamma_{xy}=-2\frac{\partial^2 w}{\partial x\partial y}z. \tag{A4}$$

Substitute Eqs. (A2) and (A4) into Eq. (A1) to obtain the components of stress

$$\begin{aligned}
&\sigma_x=-\frac{Ez}{1-\nu^2}\left(\frac{\partial^2 w}{\partial x^2}+\nu\frac{\partial^2 w}{\partial y^2}\right),\\
&\sigma_y=-\frac{Ez}{1-\nu^2}\left(\frac{\partial^2 w}{\partial y^2}+\nu\frac{\partial^2 w}{\partial x^2}\right),\\
&\tau_{xy}=-\frac{Ez}{1+\nu}\frac{\partial^2 w}{\partial x\partial y}.
\end{aligned} \tag{A5}$$

Taking moments of the stress components with respect to the x axis and the y axis, respectively, the bending moments and twisting moments with unit length can be obtained

$$\begin{aligned}
&M_x=\int_{-\delta/2}^{\delta/2}z\sigma_x dz=-D\left(\frac{\partial^2 w}{\partial x^2}+\nu\frac{\partial^2 w}{\partial y^2}\right),\\
&M_y=\int_{-\delta/2}^{\delta/2}z\sigma_y dz=-D\left(\frac{\partial^2 w}{\partial y^2}+\nu\frac{\partial^2 w}{\partial x^2}\right),\\
&M_{xy}=-M_{yx}=\int_{-\delta/2}^{\delta/2}z\tau_{xy}dz=-D(1-\nu)\frac{\partial^2 w}{\partial x\partial y}.
\end{aligned} \tag{A6}$$

A.2 Determination of differential equation of deflections (*Timoshenko 1959*)

As shown in Fig. A1(b), taking moments of all forces acting on the middle plane with respect to the x axis and the y axis, respectively, equations of equilibrium can be denoted

$$\frac{\partial M_{xy}}{\partial x}dxdy-\frac{\partial M_y}{\partial y}dydx+Q_y dxdy=0 \tag{A7}$$

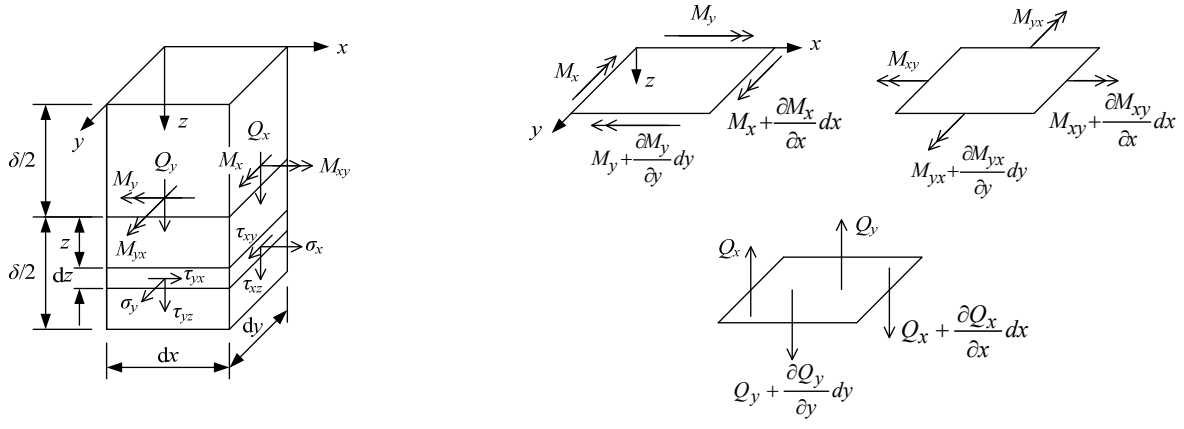

(a) (b)

Fig. A1 Moments and shearing forces in thin plates

$$\frac{\partial M_{yx}}{\partial y}dydx+\frac{\partial M_x}{\partial x}dxdy-Q_x dydx=0 \tag{A8}$$

Removing symbols *dxdy* to simplify Eqs. (A7)-(A8)

$$\frac{\partial M_{xy}}{\partial x}-\frac{\partial M_y}{\partial y}+Q_y=0 \tag{A9}$$

$$\frac{\partial M_{yx}}{\partial y}+\frac{\partial M_x}{\partial x}-Q_x=0 \tag{A10}$$

Projecting all the forces onto the *z* axis, an equation of equilibrium can be obtained

$$\frac{\partial Q_x}{\partial x}+\frac{\partial Q_y}{\partial y}+q=0 \tag{A11}$$

Substitute Eqs. (A9)-(A10) into Eq. (A11)

$$\frac{\partial^2 M_x}{\partial x^2}+\frac{\partial^2 M_y}{\partial y^2}-2\frac{\partial^2 M_{xy}}{\partial x\partial y}=-q \tag{A12}$$

The differential equation of deflections can be obtained by substituting Eq. (A6) into Eq. (A12)

$$\frac{\partial^4 w}{\partial x^4}+2\frac{\partial^4 w}{\partial x^2\partial y^2}+\frac{\partial^4 w}{\partial y^4}=\frac{q}{D} \tag{A13}$$

A.3 Rectangular plates with all edges simply supported (*Timoshenko 1959*)

A thin plate with four edges simply supported is indicated in Fig. A2(a). The boundary conditions can be summarized as

$$\begin{aligned} &(w)_{x=0}=0, && \left(\frac{\partial^2 w}{\partial x^2}\right)_{x=0}=0,\\ &(w)_{x=a}=0, && \left(\frac{\partial^2 w}{\partial x^2}\right)_{x=a}=0,\\ &(w)_{y=0}=0, && \left(\frac{\partial^2 w}{\partial y^2}\right)_{y=0}=0,\\ &(w)_{y=b}=0, && \left(\frac{\partial^2 w}{\partial y^2}\right)_{y=b}=0. \end{aligned} \tag{A14}$$

Referred to Navier solution with double trigonometric series, deflections of the plate subjected to any kind of loads can be denoted by

$$w=\sum_{m=1}^{\infty}\sum_{n=1}^{\infty}A_{mn}\sin\frac{m\pi x}{a}\sin\frac{n\pi y}{b} \tag{A15}$$

This formulation was proved to satisfy the boundary conditions in Eq. (A14) and the differential equation in Eq. (A13). Eq. (A15) was thereafter substituted into Eq. (A13) to obtain

$$\pi^4 D\sum_{m=1}^{\infty}\sum_{n=1}^{\infty}\left(\frac{m^2}{a^2}+\frac{n^2}{b^2}\right)^2 A_{mn}\sin\frac{m\pi x}{a}\sin\frac{n\pi y}{b}=q \tag{A16}$$

Expand the distributed load *q* into the double trigonometric series

$$q=\sum_{m=1}^{\infty}\sum_{n=1}^{\infty}\left(\frac{4}{ab}\int_0^a\int_0^b q\sin\frac{m\pi x}{a}\sin\frac{n\pi y}{b}dxdy\right)\times\left(\sin\frac{m\pi x}{a}\sin\frac{n\pi y}{b}\right) \tag{A17}$$

Substitute Eq. (A17) into Eq. (A16) to obtain the coefficient A_{mn}

$$A_{mn}=\frac{4\int_0^a\int_0^b q\sin\frac{m\pi x}{a}\sin\frac{n\pi y}{b}dxdy}{\pi^4 abD\left(\frac{m^2}{a^2}+\frac{n^2}{b^2}\right)^2} \tag{A18}$$

In a case that partial distributed loads were applied to the surface of the plate shown in Fig. A2(a) where the diagonal points of the loading area were (x_1, y_1) and (x_2, y_2), respectively, Eq. (A15) can be revised

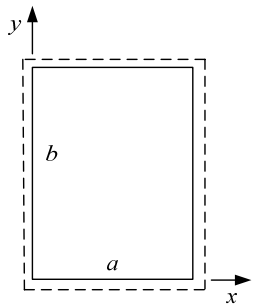

(a) Rectangular plates with four edges simply supported

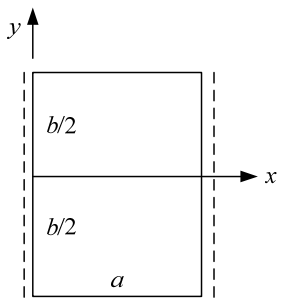

(b) Rectangular plates with two opposite edges simply supported and the other two free

Fig. A2 Rectangular plates with various edge conditions

$$w=\frac{4F}{\pi^6 D|x_2-x_1||y_2-y_1|}\times\sum_{m=1}^{\infty}\sum_{n=1}^{\infty}\frac{\left(\cos\frac{m\pi x_1}{a}-\cos\frac{m\pi x_2}{a}\right)}{mn\left(\frac{m^2}{a^2}+\frac{n^2}{b^2}\right)^2}\times\left(\cos\frac{n\pi y_1}{b}-\cos\frac{n\pi y_2}{b}\right)\times\left(\sin\frac{m\pi x}{a}\sin\frac{n\pi y}{b}\right) \tag{A19}$$

where F is the sum of the partial distributed loads.

Reactions at the corner of the plate can be calculated by the twisting moments M_{xy} as follows

$$F_R=-2M_{xy}=2D(1-\nu)\left(\frac{\partial^2 w}{\partial x\partial y}\right)=\frac{8F(1-\nu)}{\pi^4 ab|x_2-x_1||y_2-y_1|}\times\sum_{m=1}^{\infty}\sum_{n=1}^{\infty}\frac{\left(\cos\frac{m\pi x_1}{a}-\cos\frac{m\pi x_2}{a}\right)}{\left(\frac{m^2}{a^2}+\frac{n^2}{b^2}\right)^2}\times\left(\cos\frac{n\pi y_1}{b}-\cos\frac{n\pi y_2}{b}\right)\times\left(\cos\frac{m\pi x}{a}\cos\frac{n\pi y}{b}\right) \tag{A20}$$

Another case was a single load concentrated at any given point (ξ, η) of the plate. Replace distributed loads q by $F/dxdy$ to obtain new deflections

$$w=\frac{4F}{\pi^4 abD}\sum_{m=1}^{\infty}\sum_{n=1}^{\infty}\frac{\sin\frac{m\pi\xi}{a}\sin\frac{n\pi\eta}{b}}{\left(\frac{m^2}{a^2}+\frac{n^2}{b^2}\right)^2}\times\left(\sin\frac{m\pi x}{a}\sin\frac{n\pi y}{b}\right) \tag{A21}$$

A.4 Rectangular plates with two opposite edges simply supported (*Timoshenko 1959*)

A thin plate with two opposite edges simply supported and the other two edges free is indicated in Fig. A2(b). The boundary conditions can be summarized as

$$(w)_{x=0}=0,\quad\left(\frac{\partial^2 w}{\partial x^2}\right)_{x=0}=0,\qquad(w)_{x=a}=0,\quad\left(\frac{\partial^2 w}{\partial x^2}\right)_{x=a}=0,$$
$$\left(\frac{\partial^2 w}{\partial y^2}+\nu\frac{\partial^2 w}{\partial x^2}\right)_{y=\pm\frac{b}{2}}=0,\qquad\left[\frac{\partial^3 w}{\partial y^3}+(2-\nu)\frac{\partial^3 w}{\partial x^2\partial y}\right]_{y=\pm\frac{b}{2}}=0. \tag{A22}$$

The single trigonometric series with respect to the deflections of the plate subjected to distributed loads can be adopted to comply with the boundary conditions as well as the differential equation of the deflections.

$$w=\sum_{m=1}^{\infty}Y_m\sin\frac{m\pi x}{a} \tag{A23}$$

where Y_m can be expressed

$$Y_m=A_m\cosh\frac{m\pi y}{a}+B_m\frac{m\pi y}{a}\sinh\frac{m\pi y}{a}+C_m\sinh\frac{m\pi y}{a}+D_m\frac{m\pi y}{a}\cosh\frac{m\pi y}{a}+f_m(y) \tag{A24}$$

For a case that the plate was subjected to a distributed load where the location was $x=\xi$, $f_m(y)$ can be determined by

$$f_m(y)=\left(\frac{a}{m\pi}\right)^4\frac{2}{aD}\frac{F}{dx}\sin\frac{m\pi\xi}{a}dx=\frac{2Fa^3}{m^4\pi^4 D}\sin\frac{m\pi\xi}{a} \tag{A25}$$

Assume the load was applied in the symmetric axis of the plate, namely $\xi=a/2$, substitute Eq. (A23) into Eq. (A22) to obtain

$$\sum_{m=1,3,5,\cdots}^{\infty}[A_m\cosh\alpha_m+B_m(2\cosh\alpha_m+\alpha_m\sinh\alpha_m)]\times\left(\frac{m\pi}{a}\right)^2\sin\frac{m\pi x}{a}+\nu\sum_{m=1,3,5,\cdots}^{\infty}[A_m\cosh\alpha_m+B_m\alpha_m\sinh\alpha_m+\frac{2Fa^3}{m^4\pi^4 D}\sin\frac{m\pi}{2}\times\left(\frac{m\pi}{a}\right)^2\sin\frac{m\pi x}{a}=0 \tag{A26}$$

$$\sum_{m=1,3,5,\cdots}^{\infty}[A_m\sinh\alpha_m+B_m(3\sinh\alpha_m+\alpha_m\cosh\alpha_m)]\times\left(\frac{m\pi}{a}\right)^3\sin\frac{m\pi x}{a} \tag{A27}$$

$$+(2-\nu)\sum_{m=1,3,5,\cdots}^{\infty}[A_m\sinh\alpha_m + B_m(\sinh\alpha_m+\alpha_m\cosh\alpha_m)]\times\left(\frac{m\pi}{a}\right)^3\sin\frac{m\pi x}{a}=0 \tag{A27}$$

$$C_m = D_m = 0 \tag{A28}$$

Solve Eqs. (A26) and (A27) to determine the constants A_m and B_m, substitute Eqs. (A24)-(A28) into Eq. (A23) to obtain the deflections

$$w=\sum_{m=1,3,5,\cdots}^{\infty}(A_m\cosh\alpha_m + B_m\alpha_m\sinh\alpha_m + \frac{2Fa^3}{m^4\pi^4 D}\sin\frac{m\pi}{2})\times\sin\frac{m\pi x}{a} \tag{A29}$$

with

$$A_m = -\frac{2\nu Fa^3\sin\frac{m\pi}{2}}{(1+\nu)m^4\pi^4 D\cosh\alpha_m}\times\frac{\frac{5-\nu}{3-\nu}+\alpha_m\coth\alpha_m}{\frac{\nu^2-6\nu+1}{\nu^2-2\nu-3}-\alpha_m(\tanh\alpha_m-\coth\alpha_m)} \tag{A30}$$

$$B_m = \frac{2\nu Fa^3\sin\frac{m\pi}{2}}{(1+\nu)m^4\pi^4 D\cosh\alpha_m}\times\frac{1}{\frac{\nu^2-6\nu+1}{\nu^2-2\nu-3}-\alpha_m(\tanh\alpha_m-\coth\alpha_m)} \tag{A31}$$